REPORT SSD-TR-90-22

Optimization of Hydrogen Consumption in Hydrogen Masers

Prepared by

B. JADUSZLIWER and Y. C. CHAN
Chemistry and Physics Laboratory
Laboratory Operations
The Aerospace Corporation
El Segundo, CA 90245-4691

6 August 1990

Prepared for

SPACE SYSTEMS DIVISION
AIR FORCE SYSTEMS COMMAND
Los Angeles Air Force Base
P.O. Box 92960
Los Angeles, CA 90009-2960

This report was submitted by The Aerospace Corporation, El Segundo, CA 90245, under Contract No. F04701-88-C-0089 with the Space Systems Division, P. O. Box 92960, Los Angeles, CA 90009-2960. It was reviewed and approved for The Aerospace Corporation by J. M. Straus, Director, Chemistry and Physics Laboratory. Lt. Cynthia Beagle was the project officer for the Mission-Oriented Investigation and Experimentation (MOIE) Program.

This report has been reviewed by the Public Affairs Office (PAS) and is releasable to the National Technical Information Service (NTIS). At NTIS, it will be available to the general public, including foreign nationals.

This technical report has been reviewed and is approved for publication. Publication of this report does not constitute Air Force approval of the report's findings or conclusions. It is published only for the exchange and stimulation of ideas.

CYNTHIA BEAGLE, LT, USAF
MOIE Project Officer
SSD/MZSEP

JONATHAN M. EMMES, MAJ, USAF
MOIE Program Manager
AFSTC/WCO OL-AB

UNCLASSIFIED

SECURITY CLASSIFICATION OF THIS PAGE

REPORT DOCUMENTATION PAGE

1a. REPORT SECURITY CLASSIFICATION Unclassified	1b. RESTRICTIVE MARKINGS
2a. SECURITY CLASSIFICATION AUTHORITY	3. DISTRIBUTION/AVAILABILITY OF REPORT Approved for public release; distribution unlimited.
2b. DECLASSIFICATION/DOWNGRADING SCHEDULE	
4. PERFORMING ORGANIZATION REPORT NUMBER(S) TR-0090(5945-05)-2	5. MONITORING ORGANIZATION REPORT NUMBER(S) SSD-TR-90-22
6a. NAME OF PERFORMING ORGANIZATION The Aerospace Corporation Laboratory Operations 6b. OFFICE SYMBOL *(If applicable)*	7a. NAME OF MONITORING ORGANIZATION Space Systems Division
6c. ADDRESS *(City, State, and ZIP Code)* El Segundo, CA 90245-4691	7b. ADDRESS *(City, State, and ZIP Code)* Los Angeles Air Force Base Los Angeles, CA 90009-2960
8a. NAME OF FUNDING/SPONSORING ORGANIZATION 8b. OFFICE SYMBOL *(If applicable)*	9. PROCUREMENT INSTRUMENT IDENTIFICATION NUMBER F04701-88-C-0089
8c. ADDRESS *(City, State, and ZIP Code)*	10. SOURCE OF FUNDING NUMBERS PROGRAM ELEMENT NO. / PROJECT NO. / TASK NO. / WORK UNIT ACCESSION NO
11. TITLE *(Include Security Classification)* Optimization of Hydrogen Consumption in Hydrogen Masers	
12. PERSONAL AUTHOR(S) Jaduszliwer, B., and Chan, Yat C.	
13a. TYPE OF REPORT 13b. TIME COVERED FROM _____ TO _____	14. DATE OF REPORT *(Year, Month, Day)* 1990 August 6 15. PAGE COUNT 17
16. SUPPLEMENTARY NOTATION	
17. COSATI CODES FIELD / GROUP / SUB-GROUP	18. SUBJECT TERMS *(Continue on reverse if necessary and identify by block number)* Atomic clocks Hydrogen maser Hydrogen dissociator Velocity distributions Hexapole magnet

19. ABSTRACT *(Continue on reverse if necessary and identify by block number)*

Hydrogen consumption is an important reliability issue for space-qualified hydrogen masers. An excess of atoms in the upper state of the maser transition must be continuously fed into the maser bulb. Atomic hydrogen is produced in an rf discharge dissociator, and state selection is accomplished by a multipole magnet which focuses atoms in the desired state at the maser's bulb entrance orifice. The focusing properties of these magnets depend strongly on atomic speed. The quality of the match between the speed distribution of the atoms leaving the dissociator and the velocity-dependent transmission of the state selector plays an important role in determining the maser's hydrogen consumption budget. We have determined speed distributions of hydrogen atoms effusing from an rf discharge dissociator, and found that they are significantly narrower than Maxwellians. We have also performed realistic calculations of the focusing properties of hexapole magnet atomic state selectors, and explored the conditions under which good matches between atomic speed distribution and state selector transmission can be achieved.

20. DISTRIBUTION/AVAILABILITY OF ABSTRACT ☒ UNCLASSIFIED/UNLIMITED ☐ SAME AS RPT. ☐ DTIC USERS	21. ABSTRACT SECURITY CLASSIFICATION Unclassified
22a. NAME OF RESPONSIBLE INDIVIDUAL	22b. TELEPHONE *(Include Area Code)* / 22c. OFFICE SYMBOL

DD FORM 1473, 84 MAR

83 APR edition may be used until exhausted
All other editions are obsolete

SECURITY CLASSIFICATION OF THIS PAGE

UNCLASSIFIED

Preface

The authors would like to thank Dr. R. P. Frueholz for many stimulating discussions.

Contents

Figures

I. Introduction

The possibility of using hydrogen masers as frequency standards on board spacecraft requires careful consideration of long-term reliability issues. Since many of the likely failure modes of a maser involve either the atomic hydrogen source system or vacuum pump problems due to the hydrogen load, the maser's reliability will be enhanced by efficient use of its hydrogen supply.

To operate the maser, an excess of hydrogen atoms in the $F = 1$, $M = 0$ hyperfine state must be continuously fed [1] into the maser bulb. An rf discharge dissociator breaks hydrogen molecules into atoms, and the state selector (typically a hexapole or quadrupole magnet) focuses those atoms having $F = 1$, $M = 0$ at the maser's bulb entrance orifice and defocuses those having $F = 0$, $M = 0$, thus creating the population inversion required for maser operation. Clearly, the first requirement for efficient hydrogen use is that a large fraction of the hydrogen molecules flowing into the dissociator exits as atoms. But additionally there is a subtler requirement, caused by the fact that the focusing properties of the state-selecting magnet depend on the atomic velocities; since faster atoms will be deflected less than slower ones during their magnetic field traverse, the "focal length" of the magnet will be longer for those faster atoms. Thus, only atoms within a fairly narrow range of velocities will be focused at the bulb entrance orifice by a given state selector design. If there is a mismatch between the velocity distribution of the atoms coming out of the dissociator and the velocity-dependent transmission of the state selector, the hydrogen use efficiency of the maser could be seriously impaired.

Relatively little is known of the velocity distribution of atoms effusing out of rf discharge dissociators. In many cases the tacit assumption is made that the atoms will be in thermal equilibrium with the dissociator wall, but that is not necessarily the case. The threshold energy for molecular dissociation by collision with electrons in the discharge plasma is about 8.5 eV [2]. Since the molecular binding energy is only about 4.7 eV, each atom carries away approximately 2 eV of excess kinetic energy. Depending on dissociator geometry and gas density, the hydrogen atoms may, or may not, undergo enough bulk and wall collisions to thermalize fully. Velocity distributions of atoms exiting dissociators followed by cryogenically cooled thermal accommodators have been measured [3,4], but these results are not applicable to our problem since such accommodators would not be used in space-qualified masers.

We have determined the velocity distributions of hydrogen atoms effusing out of an rf discharge dissociator having a geometry and operating parameters resembling those of a maser dissociator. We have also performed realistic calculations of the velocity-dependent transmission of hexapole-magnet state selectors, investigated designs yielding good matches between atomic velocity distribution and magnet transmission, and explored the consequences of possible mismatches. This report discusses the relevant techniques and presents some results.

II. Velocity Distributions

Atomic hydrogen velocity distributions have been determined using a magnetic deflection technique described in detail elsewhere [5]. Fig. 1 shows the experimental arrangement. Hydrogen gas is fed through a temperature- controlled Pd-Ag leak [6] into a cylindrical double-walled Pyrex bulb, 15 cm long and 1.9 cm in internal diameter. Compressed-air flow between the walls provides cooling, and rf power is inductively coupled to the discharge by an external 25-turn coil. The hydrogen beam exits the dissociator through a 0.1-cm-long, 0.025-cm-wide slit, is collimated by a second slit, 0.025 cm wide, set at $d = 63.7$ cm away from the source slit, and then travels between the polepieces of an $L = 11.4$-cm-long electromagnet configured in the "two-wire" geometry described by Rabi et al. [7]. After traversing a $D = 71.3$-cm drift space, the beam is detected by a quadrupole mass analyzer. Our dissociator operates over a wide range of rf power levels and hydrogen pressures, as shown in Fig. 2; dissociation fractions of up to 80% can be achieved.

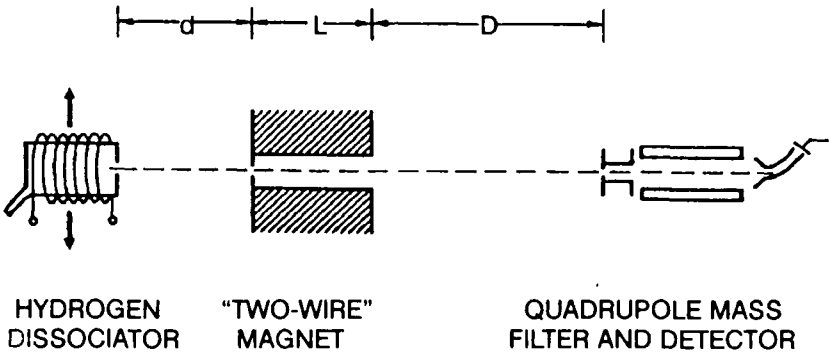

Fig. 1. Schematic view of the experimental arrangement. The hydrogen dissociator can be displaced transversely.

Molecular hydrogen, having no magnetic dipole moment, will travel through the magnet without deflection, but hydrogen atoms will be deflected by the inhomogeneous magnetic field in opposite directions depending on the sign of their magnetic moments. The dissociator is attached to the rest of the apparatus by flexible vacuum bellows, and can be displaced transversely by micrometer screws; in this way, the angular distribution of atoms deflected by the field can be measured. We have shown previously [5] that if $f_0(X)$ is the distribution of detected atoms as a function of source slit position at zero magnetic field and $g(V)$ the speed distribution of the atoms leaving the source slit, then the distribution of detected atoms when the magnetic field is turned on, $f(X)$, will be given by

$$f(X) = \sum_{F,M} \int_0^\infty f_0(X - K_{FM}/V^2)\, g(V) dV \qquad (1)$$

where

$$K_{FM} = \frac{0.492}{\alpha} \frac{\mu}{m} BLd \left(1 + \frac{d}{L + d}\right) \tag{2}$$

B is the intensity of the magnetic field, α is a magnet geometry parameter (2α is the separation of the "equivalent wires"), m is the atomic mass, and μ the effective magnetic moment of an atom having hyperfine quantum numbers F,M, given by the Breit-Rabi formula [8]. For hydrogen,

$$\mu = \pm \frac{x + M}{(1 + 2Mx + x^2)^{1/2}} \mu_0 \tag{3}$$

where μ_0 is the Bohr magneton; the (+) sign corresponds to $F=0$, $M=0$, and $F=1$, $M=-1$; the (-) sign, to $F=1$, $M=0$, and $F=1$, $M=1$. x is proportional to the ratio of magnetic-to-hyperfine energies, $x = B/(507\ \text{G})$.

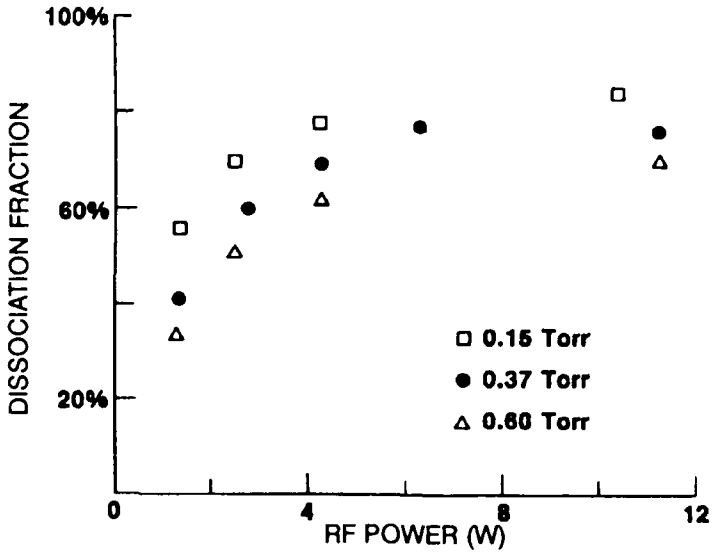

Fig. 2. Atomic hydrogen beam fraction vs rf discharge power. Total dissociator bulb pressures are indicated.

To determine the atomic speed distribution, $f_0(X)$ is measured first, and then $f(X)$ is calculated using Eq. (1) and model velocity distributions. The results of the calculations are compared with the measured $f(X)$, and the model distributions are adjusted for best fit to the experimental deflection data. Fig. 3 shows the measured undeflected beam profile $f_0(X)$, as well as the measured deflected beam profile $f(X)$ at a field of 995 G. Our technique to determine velocity distributions has been previously validated, and the apparatus has been calibrated, using an effusive rubidium beam [5]. The validation experiment showed that the left side peak in Fig. 3 should be the one used to fit the calculated deflection profile $f(X)$, since the atoms deflected into the right

side peak travel very close to the convex polepiece of the magnet, causing the constant-force approximation used in the derivation of Eq. (2) to break down.

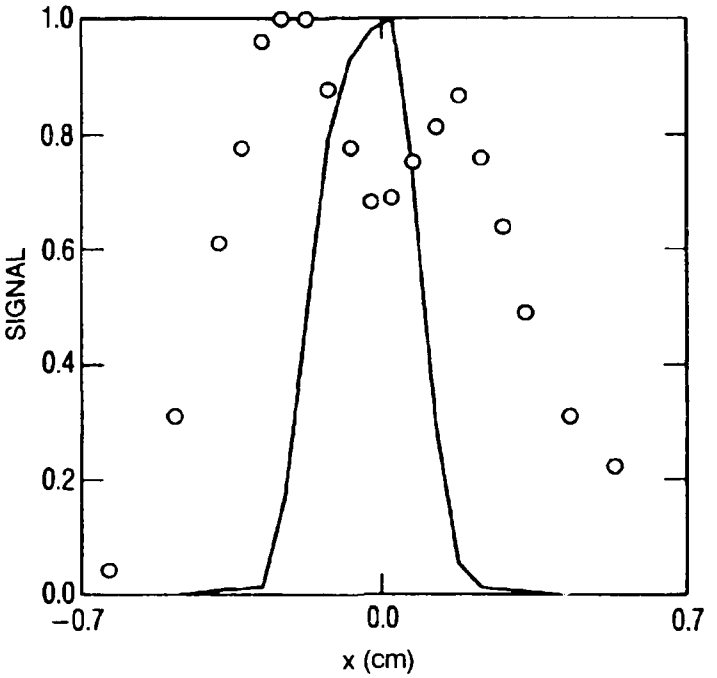

Fig. 3. Detected atomic hydrogen flux vs dissociator slit position. Full line: undeflected beam (zero field). Circles: beam defl cted by a 995-G field. Both sets of data have been normalized to unit height. Dissociator pressure: 0.058 Torr.

The analysis of preliminary atomic hydrogen deflection data showed [5] that the atomic velocity distributions are significantly narrower than Maxwellians; since then, we have obtained and analyzed additional, higher quality deflection data, and the results support that conclusion. The first model speed distribution used to generate calculated beam deflection profiles was a beam-Maxwellian:

$$g(V) = (2/V_0)(V/V_0)^3 \exp[-(V/V_0)^2] \tag{4}$$

where the most probable velocity V_0 was treated as a free parameter, since the temperature of the gas within the dissociator might be higher than the wall temperature. An example of "best fit" to the deflection data achievable using a Maxwellian distribution is shown in Fig. 4. Recalling that very fast atoms are not deflected much, and very slow atoms undergo large deflections, Fig. 4 shows that the low and high speed wings of the beam-Maxwellian distribution are both too high. We then attempted to reproduce the deflection data using a Gaussian as a model speed distribution,

$$g(V) = 1/(\sqrt{2\pi}\ \sigma) \exp[-(V - V_0)^2/2\sigma^2] \tag{5}$$

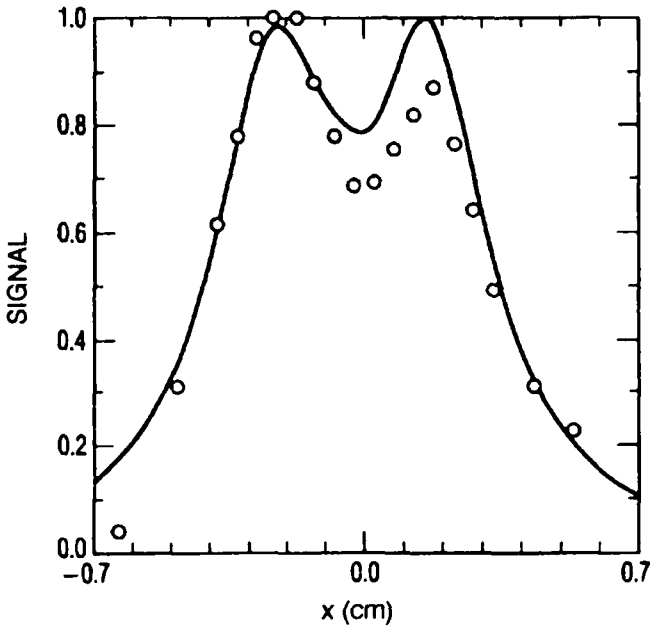

Fig. 4. Atomic hydrogen flux at detector vs dissociator slit position. Circles: as in Fig. 3. Full line: calculated for a beam-Maxwellian velocity distribution, at $T = 350$ K. Both sets of data have been normalized to unit height.

where the most probable velocity V_0 and the width σ are both treated as free parameters. This model reproduced acceptably the preliminary data [5], and fitted the new data better than the Maxwellians, but still failed to provide an acceptable match, due to the smaller error bars in the present measurements. To obtain good fits to the data, we have to allow the speed distribution to be asymmetrical. This was accomplished by using as a model distribution two half-Gaussians joined smoothly at their peaks:

$$g(V) = 1/(\sqrt{2\pi}\ \bar{\sigma})\ \exp[-\ (V - V_0)^2/2\sigma_1^2\ ] \text{ for } V < V_0 \tag{6a}$$

$$g(V) = 1/(\sqrt{2\pi}\ \bar{\sigma})\ \exp[-\ (V - V_0)^2/2\sigma_2^2\ ] \text{ for } V > V_0 \tag{6b}$$

where $\bar{\sigma} = (\sigma_1 + \sigma_2)/2$. The most probable velocity V_0 and the two partial widths σ_1 and σ_2 are treated as free parameters. With this model distribution, acceptable matches to the deflection data were obtained over the whole range of dissociator pressures we have explored. Fig. 5 illustrates the match obtained between calculated and measured deflection profiles for the same data shown in Fig. 4, and Fig. 6 shows the speed distributions used to calculate the deflection profiles in Figs. 4 and 5. It is apparent that at low dissociator pressures the atomic speed distributions are nonthermal and significantly narrower than Maxwellians.

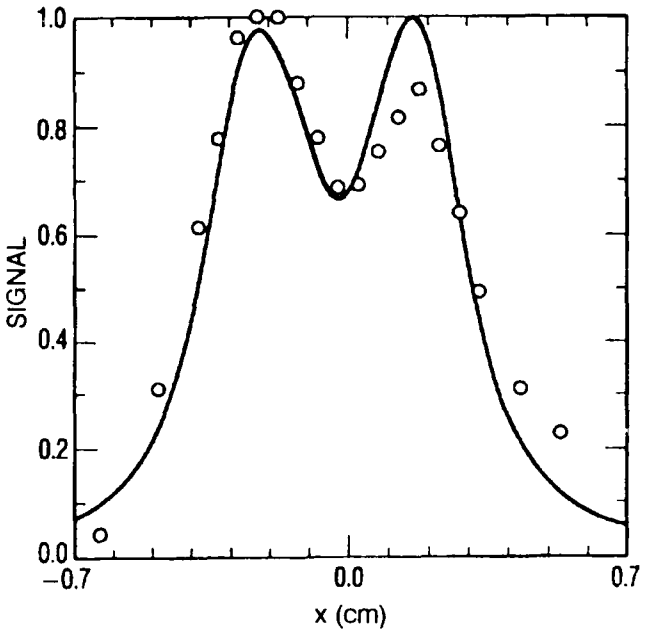

Fig. 5. Atomic hydrogen flux at detector vs dissociator slit position. Circles: as in Fig. 3. Full line: calculated for the asymmetric velocity distribution defined in the text. Both sets of data have been normalized to unit height.

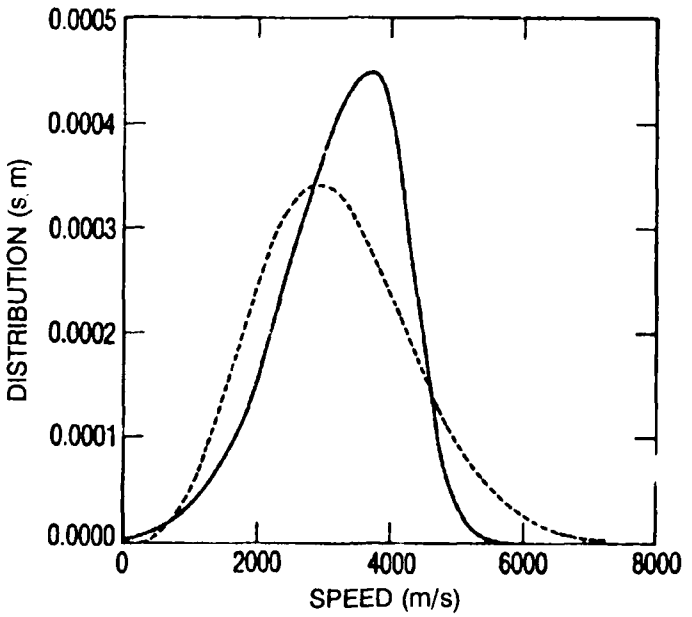

Fig. 6. Velocity distributions used to calculate the deflected beam profiles shown in Figs. 4 and 5. Full line: asymmetric distribution, as defined in text. Dashed line: beam-Maxwellian. Both curves have been normalized to unit area.

In the range of dissociator pressures we have explored (25 to 350 mTorr), neither the peak velocity nor the partial width of the distribution on the high-speed side change significantly. The dependence of the low-speed side partial width on pressure is shown in Fig. 7. At the high end of our pressure range, the overall width of the distribution is quite close to the Maxwellian width. The peak speed of the distributions corresponds to a kinetic energy of about 0.075 eV, indicating that the hydrogen atoms do lose most of their excess energy before leaving the dissociator. Since, on the other hand, the atoms do not thermalize fully, that energy loss must take place in just a few collisions, requiring a relatively high average energy loss per collision. Impact vibrational excitation of hydrogen molecules within the dissociator bulb, with an energy loss of 0.546 eV/collision, is a likely mechanism of atomic slowing-down.

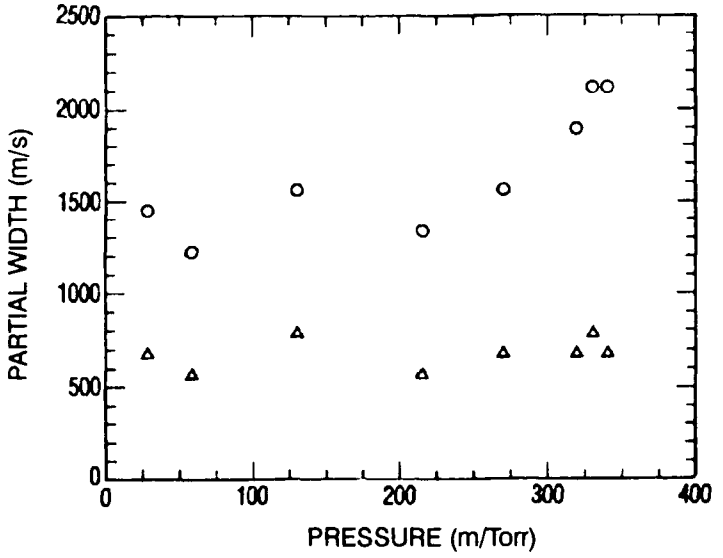

Fig. 7. Partial widths of the best-fitting asymmetric velocity distributions vs total dissociator pressure. Circles: low speed side. Triangles: high speed side.

III. Hexapole Magnets as Velocity Filters

A hexapole magnet can be used as a state selector in a hydrogen maser because the inhomogeneous hexapolar field will exert a radial force, pointed towards its axis on atoms having a negative effective magnetic moment, and outwards on atoms having a positive effective magnetic moment. In this way, for a well chosen combination of geometry and magnetic field strength, atoms having $F = 1$ and $M = 0$ can be focused at the entrance orifice of the maser bulb, while those atoms having $F = 0$, $M = 0$ will be defocused. The focusing conditions are velocity-dependent, and so the state selector will also act as a velocity filter.

The force acting on an atom immersed in an inhomogeneous magnetic field $\boldsymbol{B}$ is given by $\boldsymbol{F} = \mathrm{grad}(B)$ [9]. The effective magnetic moment, given for hydrogen by Eq. (3), will depend on the atomic quantum numbers F, M and on the magnetic field strength B. The magnetic field strength within a hexapole magnet of bore radius r_0 and poletip field B_0 is given by $B = B_0(r/r_0)^2$ [10]. The radial equation of motion for an atom within the magnet bore is then

$$\ddot{r} = (\mu/m) \times 2(B_0/r_0^2)r \tag{7}$$

where, for the $M = 0$ states of hydrogen, $\mu = \pm x/(1+x^2)^{1/2}$, and $x = (B_0/507\ \mathrm{G})(r/r_0)^2$. This equation can be rewritten in a form more suitable for numerical solution as

$$\ddot{\varrho} \pm \frac{\beta_0\, \varrho^2}{(1 + \beta_0^2\, \varrho^4)^{1/2}}\, \omega^2\, \varrho = 0 \tag{8}$$

where $\varrho = r/r_0$, $\beta_0 = B_0/(507\ \mathrm{G})$, and $\omega = (2\mu_0 B_0/m r_0^2)^{1/2}$. The solutions to this equation oscillate about the magnet axis when $\mu < 0$, and are outward bound when $\mu > 0$.

Fig. 8 shows the maser state selector geometry: a hexapole magnet of length L_2 has its entrance plane at a distance L_1 from the source exit plane; the entrance plane to the maser bulb is at a distance L_3 from the exit plane of the magnet. The axial velocity of the atom is constant. The radial velocity is constant in regions a and c, and the radial acceleration in region b is given by Eq. (7). Atomic trajectories leading from the source into the maser bulb are calculated by solving the equations of motion in regions a, b, and c, and matching radial positions and speeds at the boundary planes. The velocity-dependent transmission of the state selector can be calculated by integrating the atomic trajectories leading from source to bulb over starting coordinates and angles. Fig. 9 shows the transmission curves obtained for a given choice of parameters for atoms in both $M = 0$ states. The transmission data have been normalized to the solid angle subtended by the bulb entrance orifice, weighted by the effusive beam angular distribution (i.e., it is measured in units of the total atomic flux per unit speed that would enter the maser bulb in the absence of the magnet). For high speeds, both curves converge asymptotically to 0.25, which is the statistical

weight of each of those states. The broad transmission peak for $F = 1$ atoms at 3800 m/s contains those atoms which undergo one radial oscillation in their traverse of the magnetic field; narrower peaks at lower speeds contain atoms which undergo more radial oscillations.

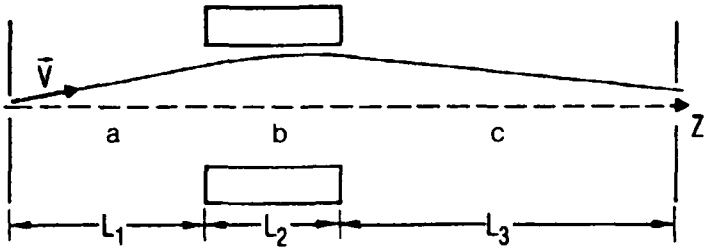

Fig. 8. Schematic view of the state selector geometry (see description in text).

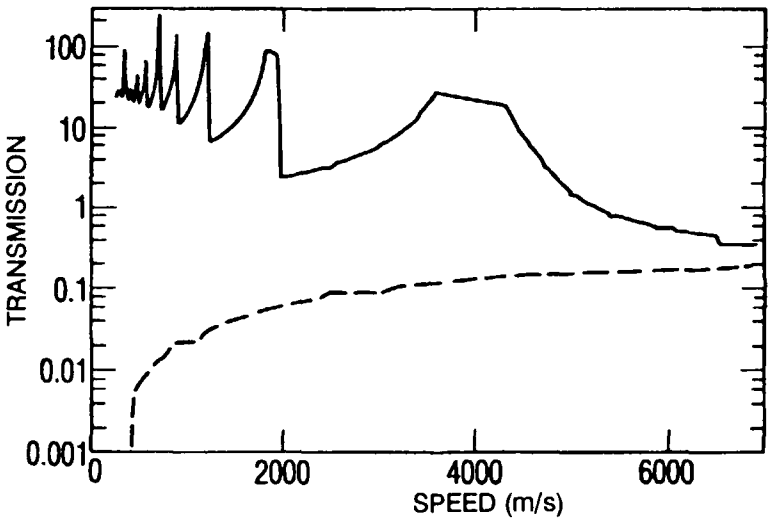

Fig. 9. Transmission of a hexapole magnet (in units of beam flux at the maser bulb entrance orifice in the absence of the magnet) vs atomic speed. Full line: $F = 1$, $M = 0$ hydrogen atoms (selected state). Dashed line: $F = 0$, $M = 0$ hydrogen atoms (rejected state).

To obtain the velocity distribution of the transmitted atoms, the velocity-dependent transmission of the magnet has to be folded with the velocity distribution of the atoms entering it. Let us assume that the atoms leaving the dissociator do so with the velocity distribution $g_0(V)$, illustrated by the full line in Fig. 6 (i.e., the distribution yielding a good fit to our beam deflection measurements). The full line in Fig. 10 shows the transmitted distribution when the magnet has been optimized for $g_0(V)$. If, on the other hand, the magnet had been optimized for a beam-Maxwellian distribution at wall temperature, the transmitted distribution would be the one shown by the dashed line in Fig. 10. Integration of the transmitted distributions over atomic speed yields the atomic fluxes into the dissociator. This procedure shows that assuming the atomic speed distri-

bution to be thermal introduces a mismatch between state selector design and atomic speed distribution which causes the waste of 65% of the $F = 1$, $M = 0$ atoms leaving the dissociator.

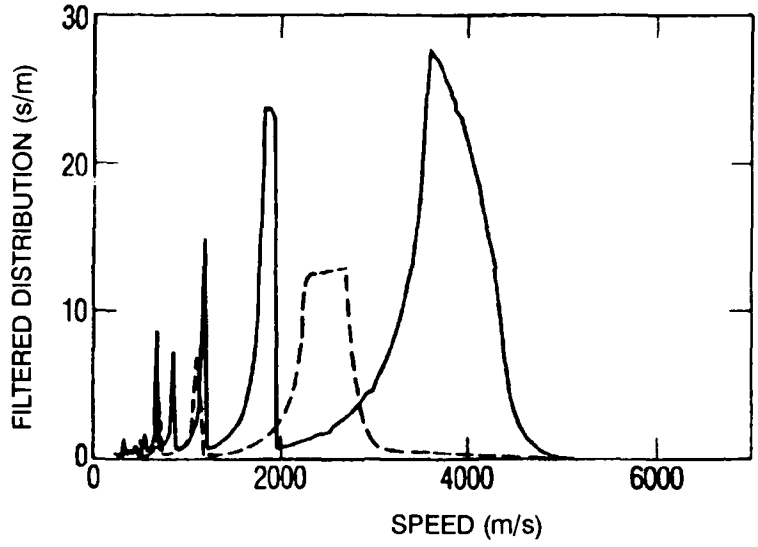

Fig. 10. Velocity distribution of the hydrogen atoms focused at the maser bulb entrance orifice. Full line: state selector optimized for the actual incident beam velocity distribution. Dashed line: state selector optimized for a Maxwellian beam at the dissociator wall temperature.

IV. Conclusions

Our studies of velocity distributions of hydrogen atoms effusing out of rf discharge have shown that while the atoms lose most of their excess kinetic energy rapidly, they may not thermalize fully before exiting. At low dissociator pressures, the atomic hydrogen beam velocity distribution is significantly narrower than the beam-Maxwellian distribution characteristic of thermal equilibrium.

Our analysis of the focusing properties of hexapole magnet state selectors shows that the efficiency of hydrogen use by the maser can be increased significantly by optimizing the state selector design for the actual atomic hydrogen velocity distribution. This finding is of particular importance for the design of space-qualified hydrogen masers, where the maser reliability is enhanced if hydrogen consumption is reduced.

References

1. D. Kleppner, H. M. Goldenberg, and N. F. Ramsey, "Theory of the Hydrogen Maser," *Phys. Rev.*, vol. 126, pp. 603–615, 1962.

2. S. J. B. Corrigan and A. Von Engel, "Excitation and Dissociation of Hydrogen by an Electron Swarm," *Proc. Roy Soc. A*, vol. 245, pp. 335–351, 1958.

3. J. T. M. Walraven and I. F. Silvera, "Helium Temperature Beam Source of Atomic Hydrogen," *Rev. Sci. Instrum.*, vol. 53, pp. 1167–1181, 1982.

4. A. Herscovitch, A. Kponou, and T. O. Niinikoski, "Cold High-Intensity Atomic Hydrogen Beam Source," *Rev. Sci. Instrum.*, vol. 58, pp. 547–556, 1987.

5. B. Jaduszliwer and Y. C. Chan, "Atomic Velocity Distributions out of Hydrogen Maser Dissociators," *Proc. 21st. PTTI Appl. and Planning Meeting*, Redondo Beach, California, 1989, pp. 223–232.

6. J. Viennet, P. Petit, and C. Audoin, "Régulateur de Débit d'Hydrogène à Réponse Rapide," *J. Phys. E*, vol. 6, pp. 257–261, 1973.

7. I. I. Rabi, J. M. B. Kellogg, and J. R. Zacharias, "The Magnetic Moment of the Proton," *Phys. Rev.*, vol 46, pp. 157–165, 1934.

8. G. Breit and I. I. Rabi, "Measurement of Nuclear Spin," *Phys. Rev,*. vol. 38, pp. 2082–2083, 1931.

9. N. F. Ramsey, *Molecular Beams.* New York: Oxford University Press, 1956, p. 89.

10. Ibid., pp. 404–407.

LABORATORY OPERATIONS

The Aerospace Corporation functions as an "architect-engineer" for national security projects, specializing in advanced military space systems. Providing research support, the corporation's Laboratory Operations conducts experimental and theoretical investigations that focus on the application of scientific and technical advances to such systems. Vital to the success of these investigations is the technical staff's wide-ranging expertise and its ability to stay current with new developments. This expertise is enhanced by a research program aimed at dealing with the many problems associated with rapidly evolving space systems. Contributing their capabilities to the research effort are these individual laboratories:

Aerophysics Laboratory: Launch vehicle and reentry fluid mechanics, heat transfer and flight dynamics; chemical and electric propulsion, propellant chemistry, chemical dynamics, environmental chemistry, trace detection; spacecraft structural mechanics, contamination, thermal and structural control; high temperature thermomechanics, gas kinetics and radiation; cw and pulsed chemical and excimer laser development, including chemical kinetics, spectroscopy, optical resonators, beam control, atmospheric propagation, laser effects and countermeasures.

Chemistry and Physics Laboratory: Atmospheric chemical reactions, atmospheric optics, light scattering, state-specific chemical reactions and radiative signatures of missile plumes, sensor out-of-field-of-view rejection, applied laser spectroscopy, laser chemistry, laser optoelectronics, solar cell physics, battery electrochemistry, space vacuum and radiation effects on materials, lubrication and surface phenomena, thermionic emission, photosensitive materials and detectors, atomic frequency standards, and environmental chemistry.

Electronics Research Laboratory: Microelectronics, solid-state device physics, compound semiconductors, radiation hardening; electro-optics, quantum electronics, solid-state lasers, optical propagation and communications; microwave semiconductor devices, microwave/millimeter wave measurements, diagnostics and radiometry, microwave/millimeter wave thermionic devices; atomic time and frequency standards; antennas, rf systems, electromagnetic propagation phenomena, space communication systems.

Materials Sciences Laboratory: Development of new materials: metals, alloys, ceramics, polymers and their composites, and new forms of carbon; nondestructive evaluation, component failure analysis and reliability; fracture mechanics and stress corrosion; analysis and evaluation of materials at cryogenic and elevated temperatures as well as in space and enemy-induced environments.

Space Sciences Laboratory: Magnetospheric, auroral and cosmic ray physics, wave-particle interactions, magnetospheric plasma waves; atmospheric and ionospheric physics, density and composition of the upper atmosphere, remote sensing using atmospheric radiation; solar physics, infrared astronomy, infrared signature analysis; effects of solar activity, magnetic storms and nuclear explosions on the earth's atmosphere, ionosphere and magnetosphere; effects of electromagnetic and particulate radiations on space systems; space instrumentation.